Development and Characterization of a *Sf-1*-Flp Mouse Model

Marco Galvan[1*], Mina Fujitani[1*], Samuel R. Heaselgrave[1], Shreya Thomas[1], Bandy Chen[1], Jenny J. Lee[1], Steven C. Wyler[1], Joel K. Elmquist[1,2,3,4#], Teppei Fujikawa[1,4,5#]

Affiliation:

1. Center for Hypothalamic Research, Department of Internal Medicine, UT Southwestern Medical Center, Dallas, Texas, USA
2. Department of Neuroscience, UT Southwestern Medical Center, Dallas, Texas, USA
3. Department of Pharmacology, UT Southwestern Medical Center, Dallas, Texas, USA
4. Peter O'Donnell Jr. Brain Institute, UT Southwestern Medical Center, Dallas, Texas, USA
5. Institute of Human Life and Ecology, Osaka Metropolitan University, Osaka, Japan

*Contribute equally

#Corresponding authors

Joel K. Elmquist

Address; Center for Hypothalamic Research, Department of Internal Medicine, UT Southwestern Medical Center, 5323 Harry Hines Blvd, Dallas, Texas 75390-9077,

Phone; +1-214-648-8609, Email; joel.elmquist@utsouthwestern.edu)

Teppei Fujikawa

Address; Center for Hypothalamic Research, Department of Internal Medicine, UT Southwestern Medical Center, 5323 Harry Hines Blvd, Dallas, Texas 75390-9077,

Phone; +1-214-648-2521, Email; teppei.fujikawa@utsouthwestern.edu

Keywords: SF-1, VMH, Flp-FRT

Disclosure: The authors have nothing to disclose.

Abstract

The use of genetically engineered tools, including combinations of Cre-LoxP and Flp-FRT systems, enable the interrogation of complex biology. Steroidogenic factor-1 (SF-1) is expressed in the ventromedial hypothalamic nucleus (VMH). Development of genetic tools, such as mice expressing Flp recombinase (Flp) in SF-1 neurons (*Sf-1*-Flp), will be useful for future studies that unravel the complex physiology regulated by the VMH. Here, we developed and characterized *Sf-1*-Flp mice and demonstrated its utility. Flp sequence was inserted into *Sf-1* locus with P2A. This insertion did not affect *Sf-1* mRNA expression levels and *Sf-1*-Flp mice do not have any visible phenotypes. They are fertile and metabolically comparable to wild-type littermate mice. Optogenetic stimulation using adeno-associated virus (AAV)-bearing Flp-dependent channelrhodopsin-2 (ChR2) increased blood glucose and skeletal muscle PGC-1α in *Sf-1*-Flp mice. This was similar to SF-1 neuronal activation using *Sf-1*-BAC-Cre and AAV-bearing Cre-dependent ChR2. Finally, we generated *Sf-1*-Flp mice that lack *β2-adrenergic receptors* (*Adrβ2*) only in skeletal muscle with a combination of Cre/LoxP technology (*Sf-1*-Flp::SKM$^{\Delta Adrβ2}$). Optogenetic stimulation of SF-1 neurons failed to increase skeletal muscle PGC-1α in *Sf-1*-Flp::SKM$^{\Delta Adrβ2}$ mice, suggesting that *Adrβ2* in skeletal muscle is *required* for augmented skeletal muscle PGC-1α by SF-1 neuronal activation. Our data demonstrate that *Sf-1*-Flp mice are useful for interrogating complex physiology.

Introduction

The ventromedial hypothalamic nucleus (VMH) regulates multiple physiological responses and has been investigated for decades (1-3). For instance, the VMH regulates metabolism, food intake, behavior such as defensive behavior, reproduction, autonomic nervous system, and many other physiological functions (1-4). Although the role of the VMH in various physiological functions is well investigated, the precise molecular and neuronal mechanisms by which the VMH regulates physiology still remain largely unclear.

Steroidogenic factor-1 (SF-1, official gene name is *Nr5a1*) is expressed in the entire VMH early in embryonic development (5-7). In adults, SF-1 expression becomes more restricted to VMH neurons in the dorsomedial and center of the VMH (5, 6). Of note, SF-1 is also expressed in the pituitary gland, adrenal gland, and gonads like the testis and ovary (8, 9). We previously demonstrated that SF-1 neurons in the VMH (VMH[SF-1] neurons) regulate skeletal muscle transcriptional events via the sympathoadrenal drive (10). Briefly, optogenetic stimulation of VMH[SF-1] neurons using *Sf-1*-BAC-Cre (11) and adeno-associated virus (AAV) that contains Cre-dependent channelrhodopsin-2 (ChR2) (AAV-DIO-ChR2) (12) increases mRNA levels of skeletal muscle *peroxisome proliferator-activated receptor gamma coactivator 1-alpha* (PGC-1α, official gene name is *Ppargc1a*) (10). Surgical ablation of the adrenal gland or global knockout of *β2-adrenergic receptors* (*Adrβ2*) hampers inductions of skeletal muscle *Pgc-1α* expression, suggesting the sympathoadrenal drives and *Adrβ2* are required for VMH[SF-1] neuronal regulation of skeletal muscle. Considering that *Adrβ2* is a major subtype of adrenergic receptors in skeletal muscle cells (13), VMH[SF-1] neurons regulate skeletal muscle PGC-1α likely via direct actions on *Adrβ2* in skeletal muscle cells. However, *Adrβ2* is expressed in other

74 metabolically important tissues, including the pancreas (14), liver (15), and VMH (16);

75 thus it is still unclear which tissues are responsible for VMH[SF-1] neuronal regulation of

76 skeletal muscle *Pgc-1α* expression when using global *Adrβ2* KO mice. To determine

77 whether *Adrβ2* in skeletal muscle cells is indeed *required* for VMH[SF-1] neurons to regulate

78 skeletal muscle PGC-1α, we needed to develop an animal model that facilitates studies

79 to ablate *Adrβ2* only in skeletal muscle cells and simultaneously to manipulate VMH[SF-1]

80 neuronal activity. To this end, we developed mice expressing Flpe recombinase (Flp) in

81 SF-1 neurons (*Sf-1*-Flp). Similar to the Cre-LoxP system, Flp recognizes FRT sites and

82 induces a variety of recombinations depending on the directions and locations of FRT

83 sites (17-20). Because there is minimum overlapping enzymatic recognition between Cre-

84 LoxP and Flp-FRT systems (21), these systems can be used in combination, enabling

85 complex genetic manipulations.

86 An insertion of Flp in *Sf-1* locus does not affect mRNA expression of *Sf-1* in the

87 hypothalamus, pituitary gland, adrenal gland, and testis/ovary where SF-1 is expressed.

88 We confirmed that *Sf-1*-Flp mice exhibit Flp activity in SF-1 neurons in the VMH without

89 any visible phenotypes. Further, fundamental metabolism such as body weight and

90 glucose levels in *Sf-1*-Flp mice is comparable to littermate wild-type control mice. By

91 crossing *Sf-1*-Flp with mice lacking *Adrβ2* only in skeletal muscle by Cre-LoxP system,

92 we achieve to activate VMH[SF-1] neurons in mice lacking *Adrβ2* only in skeletal muscle.

93 We found that lacking *Adrβ2* only in skeletal muscle cells hampers augmented skeletal

94 muscle PGC-1α by VMH[SF-1] neuronal activation. Collectively, our data demonstrate that

95 *Sf-1*-Flp mouse is a valuable tool to decipher physiology that is regulated by VMH[SF-1]

96 neurons.

Results

Generation of *Sf-1*-Flp mice

We first attempted to insert Flpe recombinase, a temperature-stabilized form of Flp (22), into the downstream of *Sf-1* coding sequence region using either IRES or P2A. However, we could not obtain any founders with either method. SF-1 global knockout is lethal in mice (23). We concluded that inserting Flp into C terminal region of SF-1 disrupted *Sf-1* transcriptional activity by some unknown mechanisms, leading to the lethality. Thus, we decided to insert Flp upstream of the start codon of *Sf-1* with P2A, which is a self-cleaving peptide (24, 25) (**SFigure 1**). Using CRISPR/Cas9 approach as we described previously (26, 27), we successfully obtained *Sf-1*-Flp mice. We bred *Sf-1*-Flp mice with Ai65f$^{TB/TB}$ mice, which bear Flp-dependent tdTomato in *Rosa26* locus (28) (*Sf-1*-Flp$^{+/-}$::Ai65f$^{TB/-}$). *Sf-1*-Flp$^{+/-}$::Ai65f$^{TB/-}$ mice expressed tdTomato in tissues where SF-1 is expressed such as the VMH, pituitary gland, adrenal gland, and gonads (**Figure 1A-F**). In the brain, tdTomato expression is restricted to the VMH and axons emanating from the VMH (**SFigure 2**). These expression patterns are consistent with previous reports (6, 29), suggesting no ectopic expression, at least in the brain. In line with previous studies (6, 11), a scatter of tdTomato-positive cells was observed outside of the VMH (**Figure 1A and B, SFigure2**). There are a couple of potential explanations for why these scatter tdTomato-positive cells were observed outside of the VMH. Although this may simply be an artifact due to the nature of transgenic animals, the following explanation is more likely the case. During embryonic development, SF-1 positive cells are migrated into the VMH from several areas such as median eminence (6). Some of these SF-1 cells during development fail to migrate into the VMH (6). Indeed, single-cell/nucleus RNA-sequence

5

120   (sc/sn-RNAseq) studies have pointed out a small number of POMC-positive cells, which

121   are located in the hypothalamic arcuate nucleus (ARH), expressing *Sf-1* (30). Further

122   studies using cutting-edge technology, such as spatial RNA-sequence (31), will be

123   warranted to determine genetic properties of these scatter cells outside of the VMH. Next,

124   we determined whether the insertion of Flp disrupts expression of *Sf-1.* We found no

125   differences in mRNA levels of *Sf-1* in the hypothalamus, pituitary gland, adrenal gland,

126   and testis/ovary between heterozygous *Sf-1*-Flp mice and wild-type littermate control

127   mice (**Figure 1G-K**). These data suggest that the insertion of Flp into 5'UTR of *Sf-1* locus

128   unlikely affects *Sf-1* mRNA expression in *Sf-1*-Flp mice.

129

130   ***Sf-1*-Flp mice have normal body weight and whole body glucose metabolism**

131   Next, we assessed baseline metabolic parameters in *Sf-1*-Flp mice by comparing

132   heterozygous *Sf-1*-Flp mice with wild-type littermate control mice. Body weight, fat mass,

133   and lean mass in *Sf-1*-Flp mice were comparable to those of control mice (**Figure 2A-H**).

134   There were no significant differences in glucose tolerance and insulin tolerance between

135   control and *Sf-1*-Flp mice (**Figure 2I, J, M, and N**). Further, fed and fast blood glucose

136   levels were comparable in control and *Sf-1*-Flp mice (**Figure 2K, L, O, and P)**, suggesting

137   that *Sf-1*-Flp mice do not have aberrant whole-body glucose metabolism. SF-1 is required

138   for maintaining normal endocrine function in mice as *Sf-1* heterozygous global knockout

139   mice exhibit aberrant blood leptin and corticosterone levels (32). Blood leptin, insulin, and

140   corticosterone levels in fed and fasting status were comparable in control and *Sf-1*-Flp

141   mice (**SFigure 3A-C**). We found that basal blood epinephrine levels in *Sf-1*-Flp male mice

142   were significantly lower than in control mice (**Figure 3A**). In female mice, blood

143   epinephrine levels tended to be lower than control mice, with the average value of

144   epinephrine in *Sf-1*-Flp female mice being approximately 55% of the control group

145   (**Figure 3C**). Blood norepinephrine levels were comparable between *Sf-1*-Flp and control

146   mice (**Figure 3B and D**), suggesting that the synthesis of epinephrine was disrupted.

147   Thus, we investigated whether epinephrine synthesis in the adrenal gland was disrupted

148   by measuring mRNA levels of tyrosine hydroxylase (*Th*), dopamine-β-hydroxylase (*dβh*),

149   and phenylethanolamine N-methyltransferase (*Pnmt*) in the adrenal gland, which are

150   essential for epinephrine synthesis. mRNA levels of *Th*, *dβh*, and *Pnmt* in male adrenal

151   glands tended to be lower than control mice (**Figure 3B-G**), and in females, they were

152   significantly lower than control mice (**Figure 3H-J**). These results suggested that the

153   synthetic pathway of epinephrine is disrupted by an insertion of P2A-Flp into the 5'-UTR

154   of *Sf-1* locus. Overall, our data demonstrated that the insertion of P2A-Flp into the 5'-UTR

155   of the *Sf-1* locus unlikely affects most SF-1 functions; however, it potentially has indirect

156   effects on adrenal medulla functions.

157

158   **Optogenetic stimulation using *Sf-1*-Flp mice**

159   Optogenetic stimulation of VMH^{SF-1} neurons using *Sf-1*-BAC-Cre mice and AAV-

160   DIO-ChR2 increases blood glucose (10, 33) and mRNA levels of PGC-1α in skeletal

161   muscle (10). Further, it suppresses appetite (34) and induces defensive behavior such as

162   burst activities that include jumping and running (4, 35). To investigate whether we can

163   utilize optogenetics in *Sf-1*-Flp mice, we delivered AAV bearing Flp-dependent ChR2

164   (AAV-fDIO-ChR2) into the VMH (*Sf-1*-Flp::ChR2) and examined whether optogenetic

165   stimulation could produce a phenocopy of the stimulation in *Sf-1*-BAC-Cre mice. The

7

166   control group received AAV that does not contain ChR2 but a fluorescent tag sequence

167   (AAV-fDIO-EYFP) (*Sf-1*-Flp::EYFP). Optogenetic stimulation of VMH^{SF-1} neurons

168   increased c-Fos in the VMH of *Sf-1*-Flp::ChR2 mice, suggesting that it is sufficient to

169   induce augmented neuronal activities in VMH^{SF-1} neurons (**Figure 4C and D**). As

170   expected, optogenetic VMH^{SF-1} neuronal activation in *Sf-1*-Flp::ChR2 mice increased

171   blood glucose (**Figure 4E**), and burst activities were observed. We confirmed that the

172   stimulation of VMH^{SF-1} neurons significantly increased blood epinephrine (**Figure 4F and**

173   **G**) and mRNA levels of *Pgc-1α* in tibial anterior (TA) skeletal muscle of *Sf-1*-Flp::ChR2

174   mice (**Figure 4H**). We further examined whether optogenetic stimulation of VMH^{SF-1}

175   neurons in *Sf-1*-Flp::ChR2 mice suppresses appetite. Mice were fasted overnight, which

176   maximized their appetite. The stimulation significantly reduced food intake even though

177   they were fasted overnight (**Figure 4I and J**). These results are a phenocopy of

178   experiments using *Sf-1*-BAC-Cre and Cre-dependent AAV containing ChR2 (10). Overall,

179   these data indicate that optogenetic tools can be used in *Sf-1*-Flp mice.

180

181   **Combination of Cre-LoxP and Flp-FRT system in *Sf-1*-Flp mice**

182   Finally, we tested whether *Adrβ2* in skeletal muscle cells is *required* for the

183   induction of skeletal muscle *Pgc-1α* mRNA by VMH^{SF-1} neuronal activation. To do so, we

184   crossed *Sf-1*-Flp to mice expressing tamoxifen-inducible Cre under the control of the

185   human skeletal muscle cell promoter (HAS-MCM) (36) and *Adrβ2* floxed (37) mice (*Sf-1*-

186   Flp::SKM^{ΔAdrβ2}). As previous studies showed (38), we confirmed that Cre activity was

187   induced in skeletal muscle of HAC-MCM mice by tamoxifen-containing (TAM) diet

188   (**SFigure 4A**). Control group was composed of littermate *Sf-1*-Flp$^{+/-}$::*Adrβ2*$^{flox/flox}$ mice

8

189   (control). All mice were fed with TAM diet. After recovery from TAM diet, AAV-fDIO-EYFP

190   or AAV-fDIO-ChR2 was microinjected into the VMH of control or *Sf-1*-Flp::SKM$^{\Delta Adr\beta2}$ mice

191   (Control::EYFP,   Control::ChR2,   *Sf-1*-Flp::SKM$^{\Delta Adr\beta2}$::EYFP,   and   *Sf-1*-

192   Flp::SKM$^{\Delta Adr\beta2}$::ChR2) (**Figure 5A**). Deletion of *Adrβ2* in skeletal muscle cells did not

193   affect increased blood glucose levels by VMH^{SF-1} neuronal activation (**Figure 5B**). In line

194   with **Figure 4**, optogenetic VMH^{SF-1} neuronal activation in Control::ChR2 mice

195   significantly increased skeletal muscle *Pgc-1α* mRNA than Control::EYFP (**Figure 5C-H**),

196   whereas deletion of *Adrβ2* in skeletal muscle cells significantly hampers augmented

197   skeletal muscle *Pgc-1α* mRNA by VMH^{SF-1} neuronal activation (**Figure 5C-H**). Of note,

198   TAM diet significantly reduced mRNA levels of *Adrβ2* in skeletal muscle of *Sf-1*-

199   Flp::SKM$^{\Delta Adr\beta2}$, but not that of control mice (**SFigure 4B**). These data demonstrate that

200   *Adrβ2* in skeletal muscle cells is *required* for augmented skeletal muscle *Pgc-1α* mRNA

201   by VMH^{SF-1} neuronal activation. In addition, these results articulate that *Sf-1*-Flp mice can

202   be used with combinations of Cre-LoxP system.

Discussion

203

204   In this study, we generate *Sf-1*-Flp mice that express Flpe recombinase in SF-1

205   cells and demonstrate that *Sf-1*-Flp mice can be useful in investigating complex

206   physiology. Our previous report indicates that *Adrβ2* contributes to VMH[SF-1] neuronal

207   regulation of skeletal muscle transcriptional events (10). However, it was unclear whether

208   VMH[SF-1] neurons regulate a direct action of *Adrβ2* in skeletal muscle cells because *Adrβ2*

209   is widely expressed throughout the body in both rodents and humans (39-41). Our current

210   study demonstrates that *Adrβ2* in skeletal muscle cells is indeed *required* for augmented

211   skeletal muscle *Pgc-1α* mRNA by VMH[SF-1] neuronal activation. This strongly suggests

212   that a direct action of *Adrβ2* in skeletal muscle cells is key for VMH[SF-1] neuronal regulation

213   of skeletal muscle transcriptional events and functions.

214   VMH[SF-1] neurons contribute to beneficial effects of exercise including reductions in

215   fat mass (42). Previous studies indicate that VMH[SF-1] neurons are key to exercise-induced

216   skeletal muscle adaptations via the sympathetic nervous system (10, 42). Our data

217   (**Figure 5**) pinpoint that *Adrβ2* in skeletal muscle cells is likely required for VMH[SF-1]

218   neurons to regulate skeletal muscle function, although further studies are needed to

219   elucidate what precise physiological functions VMH[SF-1] neurons contribute to regulate in

220   the context of long-term exercise training. These functions may include the mitochondrial

221   respiratory system and switching fiber-type composition. For instance, long-term exercise

222   training has been shown to improve mitochondrial function and alter muscle fiber-type

223   (43-45). If VMH[SF-1] neuronal activation is repeated for a certain duration (e.g., 8 to 12

224   weeks), it may enhance mitochondrial function and influence fiber-type components as

225   recurrent exercise training does.

10

226   There are a couple of technical notes to be aware of for future studies when *Sf-1*-

227   Flp mice are used. First, although we examined Flp activity in *Sf-1*-Flp mice throughout

228   the brain (**SFigure 2**), we did not survey all peripheral tissues. As the nature of genetically-

229   engineered mice, it is still possible that *Sf-1*-Flp mice may have ectopic Flp expression in

230   some tissues where endogenous SF-1 is not expressed. Further, we used tdTomato

231   expression as a surrogate of Flp activity, but it does not guarantee that Flp works with

232   other genetically-engineered tools such as transgenic mice or AAV that bear FRT sites.

233   Thus, it is important to validate each experimental model. Second, we found that *Sf-1*-Flp

234   mice have lower blood epinephrine levels (**Figure 3**). Because *Sf-1* mRNA levels in the

235   adrenal gland are comparable between *Sf-1*-Flp and control mice (**Figure 1**) and *Sf-1* is

236   only expressed in the cortex of the adrenal gland, not the medulla where catecholamines

237   are produced, it is unclear how the insertion of P2A-Flp into 5'-UTR disrupts the

238   production of epinephrine in the adrenal gland. Optogenetic studies show that *Sf-1*-Flp

239   mice can increase blood epinephrine levels by VMH^{SF-1} neuronal activation, suggesting

240   that *Sf-1*-Flp mice can modify epinephrine releases upon afferent neuronal inputs.

241   Nonetheless, we suggest that it is ideal for studies to contain a control *Sf-1*-Flp group for

242   proper interpretation of the results. Further investigations will be warranted on the

243   mechanism underlying the effects of the transgenic insertion into 5'UTR of *Sf-1* locus on

244   blood epinephrine levels in *Sf-1*-Flp mice. Third, we noticed when AAV-fDIO-ChR2 was

245   administered into the VMH of *Sf-1*-Flp mice, it took at least 5 to 6 weeks to have metabolic

246   phenotype induced by VMH^{SF-1} neuronal activation (e.g., increased glucose levels). When

247   we use *Sf-1*-BAC-Cre mice and AAV-DIO-ChR2 (10), it only takes 2 to 3 weeks to observe

248   a metabolic phenotype. The reason for these discrepancies of durations is unclear.

249   However, it is important to keep this in mind when AAV approaches are used in *Sf-1*-Flp

250   mice.

251   *Sf-1*-Flp mice will provide unique opportunities for those who investigate the

252   physiology of SF-1 cells, especially SF-1 neurons in the VMH. As shown in **Figure 5**, *Sf-*

253   *1*-Flp mice unlock the possibilities of conducting experiments that manipulate genes in

254   peripheral cells and modulate SF-1 neuronal activity or their function simultaneously.

255   Further, *Sf-1*-Flp mice can be used for temporal conditioned manipulation combined with

256   AAV approach such as using AAV bearing Flp-dependent Cre recombinase (AAV-fDIO-

257   Cre). For instance, leptin receptors (LEPR) in the VMH appear to be important in

258   regulating metabolism (11, 46), but it may be intriguing to determine the role of LEPR in

259   the VMH in adults. If AAV-fDIO-Cre is administered into the VMH of *Sf-1*-Flp mice bearing

260   two LoxP sites in LEPR locus (47) (*Sf-1*-Flp::*Lepr*$^{flox/flox}$ mice), we may be able to achieve

261   knockdown of LEPR specifically in VMH^{SF-1} neuron in adults. These approaches enable

262   circumventing potential developmental compensations that happen when conventional

263   Cre lines are used (48) and may unravel the role of interested genes in SF-1 neurons in

264   adults.

265   In addition, *Sf-1*-Flp mice will enable the investigation of the detailed function of

266   subpopulation in SF-1 neurons. Studies using sc/sn-RNAseq reveal genetically distinct

267   subpopulations of the VMH, suggesting that the VMH is an extremely heterogeneous

268   nucleus (16, 49). To interrogate which neuronal subpopulations of the VMH contribute to

269   different physiological functions, *Sf-1*-Flp mice can be valuable as it can be applied such

270   as using the INTERSECT method (21). For instance, LEPR is widely expressed in the

271   hypothalamus, including the ARH or dorsomedial hypothalamic nucleus (DMH) (50, 51).

272   The ARH and DMH are juxtaposed to the VMH, thus it is technically difficult to target

273   LEPR only in the VMH by microinjections or other injection methods. Using INTERSECT

274   method in mice expressing Flp in SF-1 neurons and Cre in LEPR-expressing neurons by

275   crossing *Sf-1*-Flp and *Lepr*-IRES-Cre mice (52), targeting LEPR neurons only in the VMH

276   can be achieved.

277   In conclusion, our data demonstrate that *Sf-1*-Flp mice can be a great asset for

278   neuroscience, metabolism, and many other fields that investigate the roles of cells

279   expressing SF-1.

13

280 **Methods**

281 **Sex as a biological variable**

282 Both male and female mice were used in Figure 1-3. Male mice were used in optogenetic

283 studies (Figure 4 and Figure 5).

284

285 **Generation of *Sf-1*-Flp mice**

286 We utilized CRISPR/Cas9 approach to generate *Sf-1*-Flp mice. The sequence of *Mus*

287 *musculus Nr5a1* (ENSMUST00000028084.5) was obtained from the Ensembl Genome

288 Database (53, 54). Exon 2 of the *Nr5a1* gene encoding the translational start sight was

289 targeted using the following guide RNA: 5'-

290 GUACGAAUAGUCCAUGCCCGGUUUUAGAGCUAUGCU-3'; For the HDR repair

291 template a 1499 bp IDT single-stranded DNA Megamer™ (Intergrated DNA Technologies,

292 US) was used encoding the Flpe recombinase sequence immediately followed by the

293 P2A self-cleaving peptide sequence (22, 25). 5' and 3' homology arms were 45 and 92

294 bp respectively. Guide RNA, trcRNA, Cas9 protein, and HDR Template (all from IDT) were

295 administered through a pronuclear injection in C57Bl/6NCrl (Charles River, US) zygotes

296 by the UT Southwestern Transgenic Technology Center. A schematic design of *Sf-1*-Flp

297 insertion was described in **SFigure 1**. Founders were screened by PCR followed by

298 Sanger sequencing. To validate Flp activity *in situ*, we bred founders with Ai65f mice that

299 express Flp-dependent tdTomato in *Rosa26* locus (28). Importantly, *Sf-1*-Flp mice will be

300 publicly available upon the materials transfer agreement between the University of Texas

301 Southwestern Medical Center (UTSW) and the recipient institute.

302

14

Genetically-engineered mice and mouse husbandry

Sf-1-Flp mice were generated as outlined above. HAS-MCM (RRID:IMSR_JAX:025750) (36), Ai65f (RRID:IMSR_JAX:032864) (28), and Ai14 (RRID:IMSR_JAX:007914) (55) mice were purchased from the Jackson Laboratory. *Abrb2* floxed mice (15) were obtained from Dr. Florent Elefteriou at Baylor College of Medicine with the permission of Dr. Gerard Karsenty at Columbia University. Ear or tail gDNA was collected from each mouse to determine its genotype. A KAPA mouse genotype kit was used for PCR genotyping (Roche, US). The sequences of genotyping primers and expected band sizes for each allele are described in **Supplemental Table 1**. Mice were housed at room temperature (22–24 ℃) with a 12 hr light/dark cycle (lights on at 6am, and 7am during daylight saving time) and fed a normal chow diet (2016 Teklad global 16% protein rodent diets, Envigo, US). Magnetic-resonance whole-body composition analyzer (EchoMRI, TX US) was used to analyze the fat and lean mass of mice. Mice were maintained in groups and singly housed after adeno-associated virus (AAV) injections and optic fiber probes insertions. Animal care was according to established NIH guidelines.

AAV injections and optic fiber probe insertions

rAAV5-nEF1α-fDIO-hChR2(H134R)-EGFP-WPRE-hGH polyA, (Catalog# PT-1384; 5.5 x 10^{12} VM/mL) and rAAV-nEF1α-fDIO-EYFP-WPRE-hGH polyA (Catalog# BHV12400246; 2.8 x 10^{12} VM/mL) were purchased from Biohippo (MD, USA). AAVs were unilaterally administered into the right side of the VMH of mice using a UMP3 UltraMicroPump (WPI, US) with 10 µL NanoFil microsyringe (WPI) and NanoFil needle (WPI; Catalog# NF33BV). The volume of AAVs was 500 nL at the rate 100 nL per minute, and the needle was left

326 for another 5 minutes after the injection was finished. The coordinates of VMH-

327 microinjection were AP; −1.4 L; +0.5, and D; −5.5 (from Bregma). The optic fiber probe

328 was inserted as following coordinates; AP; −1.4, L; +0.5, and D; −5.0. The configuration

329 of the probe was 200 μm Core, 0.39NA, Ø2.5 mm ceramic ferrule, and 6mm length (RWD

330 Life science Inc, US). The fiber probe was secured by adhesion bond (Loctite 454, Loctite

331 Inc, US). Mice were allowed to recover for at least five to six weeks after the AAV injections

332 to express recombinant proteins fully.

333

334 **Optogenetics**

335 As we previously reported (10), the laser unit (Opto engine LLC, US; Catalog# MDL-III-

336 470) was used for VMH^{SF-1} neuronal stimulations. The power of tips was set to ~1

337 mW/mm^2. The customed transistor-transistor logic generator was built based on the

338 design by the University of Colorado Optogenetics and Neural Engineering Core, which

339 is supported by the National Institute of Neurological Disorders and Stroke of the National

340 Institutes of Health under award number P30NS048154. Rotary joint patch cable

341 (Thorlabs; Catalog# RJPSF4 for LED and RJPFF4 for the laser) was used to connect to

342 the laser unit. The quick-release interconnect (Thorlabs; Catalog# ADAF2) was used to

343 connect the rotary joint patch cable to the fiber probe attached to the mouse head. The

344 stimulation was set to; 5 ms duration, 20 Hz, 2 seconds activation and 2 seconds rest

345 cycle, 30 minutes.

346

347 **Assessment of food intake**

16

348   Mice were singly housed for food intake measurement. As shown in Figure 3H, mice are

349   acclimated to time-restricted food availability for 3 days. Water was available throughout

350   acclimation and experimental days except for when 30 minutes of optogenetic stimulation

351   was executed. Food was available between ZT5 to ZT10. On the experimental day, mice

352   were moved to the experimental cages without food. After optogenetic stimulation was

353   finished at ZT5, food and water were provided. Food weight was measured at 30, 60, and

354   120 minutes.

355

356   **Immunohistochemistry and Fos counting**

357   Mouse brains were prepared as previously described (10, 56). Anti-c-Fos (Abcam, US;

358   Catalog# ab190289, Lot# GR3418522-1, and RRID:AB_2737414) and secondary

359   fluorescent antibodies (Thermo Fisher Scientific, Inc, US; Catalog# A-21203,

360   Lot#WD319534, and RRID:AB_141633) were used. Dilution factors for antibodies were

361   1:2000 for the primary and 1:200 for the secondary antibodies. Images were captured by

362   a fluorescence microscopy (Leica Inc, US; Model DM6 B) or a slide scanner (Axioscan 7;

363   (Zeiss US, US). Quantification of c-Fos-positive cells was described previously (10).

364   Briefly, the exposure of captured images was adjusted and the VMH region was clipped

365   by Photoshop based on the mouse brain atlas [28]. Clipped images were exported to Fiji,

366   and the number of cells expressing Fos was counted by particle measurement function.

367

368   **Assessment of glucose, catecholamines, and hormone levels in the blood**

369   Blood glucose was measured by a glucose meter as previously described (42, 57, 58).

370   Blood for leptin, insulin, and corticosterone measurement was collected by tail-nicking

17

371 with a heparin-coated capillary glass tube. We removed food 2 hours before blood

372 collection to avoid immediate postprandial effects on blood metabolite and hormone and

373 defined this condition as fed status in this study. For catecholamine measurement, trunk

374 blood (**Figure 3A**) or submandibular blood (**Figure 4F**) was used. Plasma

375 catecholamines and hormone levels were measured as previously described (42, 58).

376 Briefly, the plasma catecholamines were analyzed by the Vanderbilt Hormone Assay &

377 Analytical Services Core. Plasma leptin (Crystal Chem Inc, US; Catalog# 90030 and

378 RRID:AB_2722664), insulin (Crystal Chem Inc, US; Catalog# 90080 and

379 RRID:AB_2783626), and corticosterone (Cayman Chemical, US; Catalog #501320 and

380 RRID:AB_2868564) levels were determined by commercially available ELISA kits.

381

382 **Glucose and Insulin tolerance tests**

383 For glucose tolerance test, mice were fasted for 6 hours prior to testing starting at ZT2

384 with water provided ad libitum. For the glucose tolerance test, mice received an

385 intraperitoneal injection of glucose solution (2 g/kg per BW). Glucose solution was

386 purchased from ThermoFisher (catalog # A2494001). For insulin tolerance test, mice

387 were fasted for 4 hours prior to testing starting at ZT4 with water provided ad libitum. Mice

388 received i.p. insulin (Humalin® R, Eli Lilly, US) at 0.75 U/kg per BW for male mice and

389 0.50 U/kg per BW for female mice. Blood glucose was measured using a handheld

390 glucometer (Bayer's Contour Blood Glucose Monitoring System; Leverkusen Germany).

391

392 **Assessment of mRNA**

393   mRNA levels in tissues were determined as previously described (42, 59). The sequences

394   of primers for qPCR using SYBR or the catalog of Taqman probes are described

395   previously (60) and in **Supplemental Table 2**.

396

397   **Graphic software, Data analysis, and statistical design**

398   The schematic design of *Sf-1*-Flp mice in **Supplemental Figure 1** was generated by

399   SnapGene (GSL Biotech LLC, US). The data are represented as means ± S.E.M.

400   GraphPad PRISM version 10 (GraphPad, US) was used for the statistical analyses and

401   *P*<0.05 was considered as a statistically significant difference. A detailed analysis of each

402   figure was described in **Supplemental Table 3**. The sample size was decided based on

403   previous publications (26, 42, 56-59, 61-63), and no power analysis was used. Figures

404   were generated using PRISM version 10, Illustrator 2023 and 2025, and Photoshop 2023

405   and 2025 (Adobe Inc, US).

406

407   **Study approval**

408   All procedures using mice were approved by the Institutional Animal Care and Use

409   Committee of UTSW, and animal experiments were performed at UTSW.

410

411   **Data availability**

412   All datasets generated during the current study are provided in **the Supporting Data**

413   **Values File**.

Acknowledgment

Contribution

M.G. and M.F. designed, performed, and analyzed experiments, and edited the manuscript. M.G. and M.F. equally contributed to this study, and they have the right to list them as the first author. S.R.H., S.T., B.C., and J.J.L. performed experiments. S.C.W designed *Sf-1*-Flp materials such as gRNA and edited the manuscript. J.K.E. supervised and edited the manuscript. T.F. designed, performed, supervised, and analyzed experiments, and wrote and finalized the manuscript.

Figure Legends

Figure 1. Generation of *Sf-1*-Flp mice. The representative figures of (**A and B**) the ventromedial hypothalamic nucleus (VMH), (**C**) pituitary gland, (**D**) adrenal gland, (**E**) the testis, and (**F**) ovary of *Sf-1*-Flp::Ai65f mice. Ai65f mice bearing Flp-dependent tdTomato in *Rosa26* locus. All white scale bars are 500 µm. mRNA levels of *Sf-1* in the (**G**) hypothalamus, (**H**) pituitary gland, (**I**) adrenal gland, (**J**) the testis in males, and (**K**) ovary in female of *Sf-1*-Flp heterozygous mice. The control group is composed of wild-type littermate mice. Values are mean ± S.E.M.

Figure 2. *Sf-1*-Flp mice do not have aberrant body weight and glucose metabolism. The time course of body weight of *Sf-1*-Flp heterozygous (**A**) male and (**E**) female mice. (**B, F**) Body weight, (**C, G**) fat mass, and (**D, H**) lean mass in fed and 24-hour fast conditions in *Sf-1*-Flp heterozygous (**B-D**) male and (**F-H**) female mice. Glucose tolerance test in *Sf-1*-Flp heterozygous (**I**) male and (**M**) female mice. Insulin tolerance test in *Sf-1*-Flp heterozygous (**J**) male and (**N**) female mice. Blood glucose levels in fed and 24-hour fast conditions in *Sf-1*-Flp heterozygous (**K and L**) male and (**O and P**) female mice. Values are mean ± S.E.M. Detailed statical analysis was described in Supplemetal Table 3.

Figure 3. *Sf-1*-Flp mice have lower blood epinephrine. (A-D) Blood catecholamine levels in fed and 24-hour fast conditions in *Sf-1*-Flp heterozygous male and female mice. (**B-J**) mRNA levels of tyrosine hydroxylase (*Th*), dopamine-β-hydroxylase (*dβh*), and

453   phenylethanolamine N-methyltransferase (*Pnmt*) in the adrenal gland in *Sf-1*-Flp

454   heterozygous male and female mice. Values are mean ± S.E.M. *** p < 0.001, ** p <0.01,

455   * p < 0.05.

456

457   **Figure 4. Optogenetic activation of VMH^{SF-1} neurons using *Sf-1*-Flp mice.** (**A**)

458   Schematic figure of targeting site of VMH^{SF-1} neurons using *Sf-1*-Flp mice and AAV

459   containing Flp-dependent ChR2. (**B**) Experimental design and stimulus setting of

460   optogenetics. (**C**) Representative figures of c-Fos expression pattern in the hypothalamus

461   of mice expressing EGFP (*Sf-1*-Flp::EYFP) or ChR2 (*Sf-1*-Flp::ChR2) in VMH^{SF-1} neurons

462   after optogenetic stimulation. (**D**) Number of c-Fos positive cells in the VMH of *Sf-1*-

463   Flp::ChR2 mice after optogenetic stimulation. (**E**) Blood glucose levels in *Sf-1*-Flp::ChR2

464   mice with optogenetic stimulation. (**F and G**) Blood catecholamine levels and (**H**) mRNA

465   expression levels of *Pgc1*-α isoform in skeletal muscle of *Sf-1*-Flp::ChR2 mice after

466   optogenetic stimulation. (**I**) Experimental design for food intake study. (**J**) Food intake in

467   *Sf-1*-Flp::ChR2 mice with optogenetic stimulation. All mice were male. Values are mean

468   ± S.E.M. *** p < 0.001, ** p <0.01, * p < 0.05.

469

470   **Figure 5. *Adrβ2* in skeletal muscle cells is *required* for augmented skeletal muscle**

471   **PGC-1α mRNA by VMH^{SF-1} neuronal activation.** (**A**) Experimental design to generate

472   mice lacking *Adrb2* in skeletal muscle cells (*Sf-1*-Flp::SKM^{ΔAdrβ2}) and expressing ChR2 in

473   VMH^{SF-1} neurons (*Sf-1*-Flp::SKM^{ΔAdrβ2}::ChR2). AAV-fDIO-EYFP was used as control-AAV

474   for AAV-fDIO-ChR2 (*Sf-1*-Flp::SKM^{ΔAdrβ2}::EYFP). Control group that do not lack *Adrb2* in

475   skeletal muscle cells (control) was also administered either AAV-fDIO-EYFP or AAV-fDIO-

22

476   ChR2 (Control::EYFP or Control::ChR2).   (**B**) Blood glucose levels of *Sf-1-*

477   Flp::SKM$^{\Delta Adr\beta2}$::ChR2 mice after optgenetic stimulation. (**C-H**) mRNA expression levels of

478   *Pgc1*-α isoform in skeletal muscle of *Sf-1*-Flp::SKM$^{\Delta Adr\beta2}$::ChR2 mice after optogenetic

479   stimulation. All mice were male. Values are mean ± S.E.M. *** $p < 0.001$, * $p < 0.05$.

480 **Supplemental Figure Legends**

481

482 **Supplemental Figure 1. The schematic design of *Sf-1*-Flp mice**. WT allele (upper) and

483 *Sf-1*-Flp allele (lower) sequences are described. SF-1-Flp_F1, F2, and R3 indicate the

484 location of genotype primers for *Sf-1*-Flp mice.

485

486 **Supplemental Figure 2. Brains sections of *Sf-1*-Flp::Ai65f$^{TB/-}$ mice.** Blue color

487 indicates DAPI staining and red color indicates SF-1 positive cells.

488

489 **Supplemental Figure 3. *Sf-1*-Flp mice have normal responses of corticosterone,**

490 **leptin, and insulin to fasting challenge.** Blood (**A**) corticosterone, (**B**) insulin, (**C**) and

491 leptin levels in fed and 24-hour fast conditions in *Sf-1*-Flp heterozygous male and female

492 mice. Values are mean ± S.E.M.

493

494 **Supplemental Figure 4. *Sf-1*-Flp::SKM$^{\Delta Adr\beta2}$ mice has lower Adrb2 mRNA**

495 **expression in skeletal muscle.** (**A**) Representative figure of lower limbs of HAC-

496 MCM::Ai14$^{TB/-}$ mice after 4 weeks tamoxifen (TAM) diet. A control group is composed of

497 Ai14 mice. All mice were fed with 4 weeks TAM diet. (**B**) mRNA levels of *Adrb2* in TA

498 skeletal muscle in *Sf-1*-Flp::SKM$^{\Delta Adr\beta2}$ mice after 4 weeks tamoxifen diet. A control group

499 is composed of *Sf-1*-Flp$^{+/-}$::*Adrβ2*$^{flox/flox}$ mice. All mice were fed with 4 weeks TAM diet.

500 Values are mean ± S.E.M. **** p < 0.0001

References

1. Tu L, Fukuda M, Tong Q, and Xu Y. The ventromedial hypothalamic nucleus: watchdog of whole-body glucose homeostasis. *Cell Biosci.* 2022;12(1):71.

2. Choi YH, Fujikawa T, Lee J, Reuter A, and Kim KW. Revisiting the Ventral Medial Nucleus of the Hypothalamus: The Roles of SF-1 Neurons in Energy Homeostasis. *Front Neurosci.* 2013;7:71.

3. King BM. The rise, fall, and resurrection of the ventromedial hypothalamus in the regulation of feeding behavior and body weight. *Physiology & behavior.* 2006;87(2):221-44.

4. Kunwar PS, Zelikowsky M, Remedios R, Cai H, Yilmaz M, Meister M, et al. Ventromedial hypothalamic neurons control a defensive emotion state. *Elife.* 2015;4.

5. McClellan KM, Parker KL, and Tobet S. Development of the ventromedial nucleus of the hypothalamus. *Frontiers in neuroendocrinology.* 2006;27(2):193-209.

6. Cheung CC, Kurrasch DM, Liang JK, and Ingraham HA. Genetic labeling of SF-1 neurons in mice reveals VMH circuitry beginning at neurogenesis and development of a separate non-SF-1 neuronal cluster in the ventrolateral VMH. *The Journal of comparative neurology.* 2012.

7. Ikeda Y, Luo X, Abbud R, Nilson JH, and Parker KL. The nuclear receptor steroidogenic factor 1 is essential for the formation of the ventromedial hypothalamic nucleus. *Mol Endocrinol.* 1995;9(4):478-86.

8. Zhao L, Bakke M, Krimkevich Y, Cushman LJ, Parlow AF, Camper SA, et al. Steroidogenic factor 1 (SF1) is essential for pituitary gonadotrope function. *Development.* 2001;128(2):147-54.

9. Parker KL, Rice DA, Lala DS, Ikeda Y, Luo X, Wong M, et al. Steroidogenic factor 1: an essential mediator of endocrine development. *Recent Prog Horm Res.* 2002;57:19-36.

10. Yoshida T, Fujitani M, Farmer S, Harada A, Shi Z, Lee JJ, et al. VMHdm/c(SF-1) Neuronal Circuits Regulate Skeletal Muscle PGC1-alpha via the Sympathoadrenal Drive. *Mol Metab.* 2023:101792.

11. Dhillon H, Zigman JM, Ye C, Lee CE, McGovern RA, Tang V, et al. Leptin directly activates SF1 neurons in the VMH, and this action by leptin is required for normal body-weight homeostasis. *Neuron.* 2006;49(2):191-203.

12. Fenno L, Yizhar O, and Deisseroth K. The development and application of optogenetics. *Annu Rev Neurosci.* 2011;34:389-412.

13. Lynch GS, and Ryall JG. Role of beta-adrenoceptor signaling in skeletal muscle: implications for muscle wasting and disease. *Physiol Rev.* 2008;88(2):729-67.

14. Ceasrine AM, Lin EE, Lumelsky DN, Iyer R, and Kuruvilla R. Adrb2 controls glucose homeostasis by developmental regulation of pancreatic islet vasculature. *Elife.* 2018;7.

15. Ghosh PM, Shu ZJ, Zhu B, Lu Z, Ikeno Y, Barnes JL, et al. Role of beta-adrenergic receptors in regulation of hepatic fat accumulation during aging. *J Endocrinol.* 2012;213(3):251-61.

16. Steuernagel L, Lam BYH, Klemm P, Dowsett GKC, Bauder CA, Tadross JA, et al. HypoMap-a unified single-cell gene expression atlas of the murine hypothalamus. *Nat Metab.* 2022;4(10):1402-19.

17. Andrews BJ, Proteau GA, Beatty LG, and Sadowski PD. The FLP recombinase of the 2 micron circle DNA of yeast: interaction with its target sequences. *Cell.* 1985;40(4):795-803.

18. O'Gorman S, Fox DT, and Wahl GM. Recombinase-mediated gene activation and site-specific integration in mammalian cells. *Science.* 1991;251(4999):1351-5.

19. Andrews BJ, Beatty LG, and Sadowski PD. Isolation of intermediates in the binding of the FLP recombinase of the yeast plasmid 2-micron circle to its target sequence. *J Mol Biol.* 1987;193(2):345-58.

20. Branda CS, and Dymecki SM. Talking about a revolution: The impact of site-specific recombinases on genetic analyses in mice. *Dev Cell.* 2004;6(1):7-28.

21. Fenno LE, Mattis J, Ramakrishnan C, Hyun M, Lee SY, He M, et al. Targeting cells with single vectors using multiple-feature Boolean logic. *Nat Methods.* 2014;11(7):763-72.

22. Buchholz F, Angrand PO, and Stewart AF. Improved properties of FLP recombinase evolved by cycling mutagenesis. *Nat Biotechnol.* 1998;16(7):657-62.

23. Luo X, Ikeda Y, and Parker KL. A cell-specific nuclear receptor is essential for adrenal and gonadal development and sexual differentiation. *Cell.* 1994;77(4):481-90.

24. Szymczak AL, Workman CJ, Wang Y, Vignali KM, Dilioglou S, Vanin EF, et al. Correction of multi-gene deficiency in vivo using a single 'self-cleaving' 2A peptide-based retroviral vector. *Nat Biotechnol.* 2004;22(5):589-94.

25. Kim JH, Lee SR, Li LH, Park HJ, Park JH, Lee KY, et al. High cleavage efficiency of a 2A peptide derived from porcine teschovirus-1 in human cell lines, zebrafish and mice. *PLoS One.* 2011;6(4):e18556.

26. Castorena CM, Caron A, Michael NJ, Ahmed NI, Arnold AG, Lee J, et al. CB1Rs in VMH neurons regulate glucose homeostasis but not body weight. *Am J Physiol Endocrinol Metab.* 2021;321(1):E146-e55.

27. Wyler SC, Gahlot S, Bideyan L, Yip C, Dushime J, Chen B, et al. LCoRL regulates growth and metabolism. *Endocrinology.* 2024.

28. Daigle TL, Madisen L, Hage TA, Valley MT, Knoblich U, Larsen RS, et al. A Suite of Transgenic Driver and Reporter Mouse Lines with Enhanced Brain-Cell-Type Targeting and Functionality. *Cell.* 2018;174(2):465-80 e22.

29. Lindberg D, Chen P, and Li C. Conditional viral tracing reveals that steroidogenic factor 1-positive neurons of the dorsomedial subdivision of the ventromedial hypothalamus project to autonomic centers of the hypothalamus and hindbrain. *J Comp Neurol.* 2013;521(14):3167-90.

30. Yu H, Rubinstein M, and Low MJ. Developmental single-cell transcriptomics of hypothalamic POMC neurons reveal the genetic trajectories of multiple neuropeptidergic phenotypes. *Elife.* 2022;11.

31. Marx V. Method of the Year: spatially resolved transcriptomics. *Nat Methods.* 2021;18(1):9-14.

32. Bland ML, Jamieson CA, Akana SF, Bornstein SR, Eisenhofer G, Dallman MF, et al. Haploinsufficiency of steroidogenic factor-1 in mice disrupts adrenal

590   development leading to an impaired stress response. *Proc Natl Acad Sci U S A.*
591   2000;97(26):14488-93.

592 33. Meek TH, Matsen ME, Damian V, Cubelo A, Chua SC, Jr., and Morton GJ. Role of
593   melanocortin signaling in neuroendocrine and metabolic actions of leptin in male
594   rats with uncontrolled diabetes. *Endocrinology.* 2014;155(11):4157-67.

595 34. Zhang J, Chen D, Sweeney P, and Yang Y. An excitatory ventromedial
596   hypothalamus to paraventricular thalamus circuit that suppresses food intake. *Nat*
597   *Commun.* 2020;11(1):6326.

598 35. Wang L, Chen IZ, and Lin D. Collateral pathways from the ventromedial
599   hypothalamus mediate defensive behaviors. *Neuron.* 2015;85(6):1344-58.

600 36. McCarthy JJ, Srikuea R, Kirby TJ, Peterson CA, and Esser KA. Inducible Cre
601   transgenic mouse strain for skeletal muscle-specific gene targeting. *Skelet Muscle.*
602   2012;2(1):8.

603 37. Kajimura D, Hinoi E, Ferron M, Kode A, Riley KJ, Zhou B, et al. Genetic
604   determination of the cellular basis of the sympathetic regulation of bone mass
605   accrual. *J Exp Med.* 2011;208(4):841-51.

606 38. Meister J, Bone DBJ, Knudsen JR, Barella LF, Velenosi TJ, Akhmedov D, et al.
607   Clenbuterol exerts antidiabetic activity through metabolic reprogramming of
608   skeletal muscle cells. *Nat Commun.* 2022;13(1):22.

609 39. Kim MS, Pinto SM, Getnet D, Nirujogi RS, Manda SS, Chaerkady R, et al. A draft
610   map of the human proteome. *Nature.* 2014;509(7502):575-81.

611 40. Thul PJ, and Lindskog C. The human protein atlas: A spatial map of the human
612   proteome. *Protein Sci.* 2018;27(1):233-44.

613 41. Wu C, Orozco C, Boyer J, Leglise M, Goodale J, Batalov S, et al. BioGPS: an
614   extensible and customizable portal for querying and organizing gene annotation
615   resources. *Genome Biol.* 2009;10(11):R130.

616 42. Fujikawa T, Castorena CM, Pearson M, Kusminski CM, Ahmed N, Battiprolu PK,
617   et al. SF-1 expression in the hypothalamus is required for beneficial metabolic
618   effects of exercise. *Elife.* 2016;5.

619 43. Hawley JA, Hargreaves M, Joyner MJ, and Zierath JR. Integrative biology of
620   exercise. *Cell.* 2014;159(4):738-49.

621 44. Pedersen BK, and Saltin B. Exercise as medicine - evidence for prescribing
622   exercise as therapy in 26 different chronic diseases. *Scand J Med Sci Sports.*
623   2015;25 Suppl 3:1-72.

624 45. Egan B, and Zierath JR. Exercise metabolism and the molecular regulation of
625   skeletal muscle adaptation. *Cell Metab.* 2013;17(2):162-84.

626 46. Jacob RJ, Dziura J, Medwick MB, Leone P, Caprio S, During M, et al. The effect of
627   leptin is enhanced by microinjection into the ventromedial hypothalamus. *Diabetes.*
628   1997;46(1):150-2.

629 47. Balthasar N, Coppari R, McMinn J, Liu SM, Lee CE, Tang V, et al. Leptin receptor
630   signaling in POMC neurons is required for normal body weight homeostasis.
631   *Neuron.* 2004;42(6):983-91.

632 48. Song AJ, and Palmiter RD. Detecting and Avoiding Problems When Using the Cre-
633   lox System. *Trends Genet.* 2018;34(5):333-40.

49. Affinati AH, Sabatini PV, True C, Tomlinson AJ, Kirigiti M, Lindsley SR, et al. Cross-species analysis defines the conservation of anatomically segregated VMH neuron populations. *Elife.* 2021;10.

50. Scott MM, Lachey JL, Sternson SM, Lee CE, Elias CF, Friedman JM, et al. Leptin targets in the mouse brain. *The Journal of comparative neurology.* 2009;514(5):518-32.

51. Elmquist JK, Bjorbaek C, Ahima RS, Flier JS, and Saper CB. Distributions of leptin receptor mRNA isoforms in the rat brain. *The Journal of comparative neurology.* 1998;395(4):535-47.

52. DeFalco J, Tomishima M, Liu H, Zhao C, Cai X, Marth JD, et al. Virus-assisted mapping of neural inputs to a feeding center in the hypothalamus. *Science.* 2001;291(5513):2608-13.

53. Hubbard T, Barker D, Birney E, Cameron G, Chen Y, Clark L, et al. The Ensembl genome database project. *Nucleic Acids Res.* 2002;30(1):38-41.

54. Harrison PW, Amode MR, Austine-Orimoloye O, Azov AG, Barba M, Barnes I, et al. Ensembl 2024. *Nucleic Acids Res.* 2024;52(D1):D891-D9.

55. Madisen L, Zwingman TA, Sunkin SM, Oh SW, Zariwala HA, Gu H, et al. A robust and high-throughput Cre reporting and characterization system for the whole mouse brain. *Nat Neurosci.* 2010;13(1):133-40.

56. Fujikawa T, Berglund ED, Patel VR, Ramadori G, Vianna CR, Vong L, et al. Leptin engages a hypothalamic neurocircuitry to permit survival in the absence of insulin. *Cell Metab.* 2013;18(3):431-44.

57. Singha AK, Yamaguchi J, Gonzalez NS, Ahmed N, Toney GM, and Fujikawa T. Glucose-Lowering by Leptin in the Absence of Insulin Does Not Fully Rely on the Central Melanocortin System in Male Mice. *Endocrinology.* 2019;160(3):651-63.

58. Singha A, Palavicini JP, Pan M, Farmer S, Sandoval D, Han X, et al. Leptin Receptors in RIP-Cre(25Mgn) Neurons Mediate Anti-dyslipidemia Effects of Leptin in Insulin-Deficient Mice. *Front Endocrinol (Lausanne).* 2020;11:588447.

59. Fujikawa T, Chuang JC, Sakata I, Ramadori G, and Coppari R. Leptin therapy improves insulin-deficient type 1 diabetes by CNS-dependent mechanisms in mice. *Proc Natl Acad Sci U S A.* 2010;107(40):17391-6.

60. Ruas JL, White JP, Rao RR, Kleiner S, Brannan KT, Harrison BC, et al. A PGC-1alpha isoform induced by resistance training regulates skeletal muscle hypertrophy. *Cell.* 2012;151(6):1319-31.

61. Miyaki T, Fujikawa T, Kitaoka R, Hirano N, Matsumura S, Fushiki T, et al. Noradrenergic projections to the ventromedial hypothalamus regulate fat metabolism during endurance exercise. *Neuroscience.* 2011;190:239-50.

62. Asterholm IW, Rutkowski JM, Fujikawa T, Cho YR, Fukuda M, Tao C, et al. Elevated resistin levels induce central leptin resistance and increased atherosclerotic progression in mice. *Diabetologia.* 2014;57(6):1209-18.

63. Williams KW, Liu T, Kong X, Fukuda M, Deng Y, Berglund ED, et al. Xbp1s in Pomc neurons connects ER stress with energy balance and glucose homeostasis. *Cell Metab.* 2014;20(3):471-82.
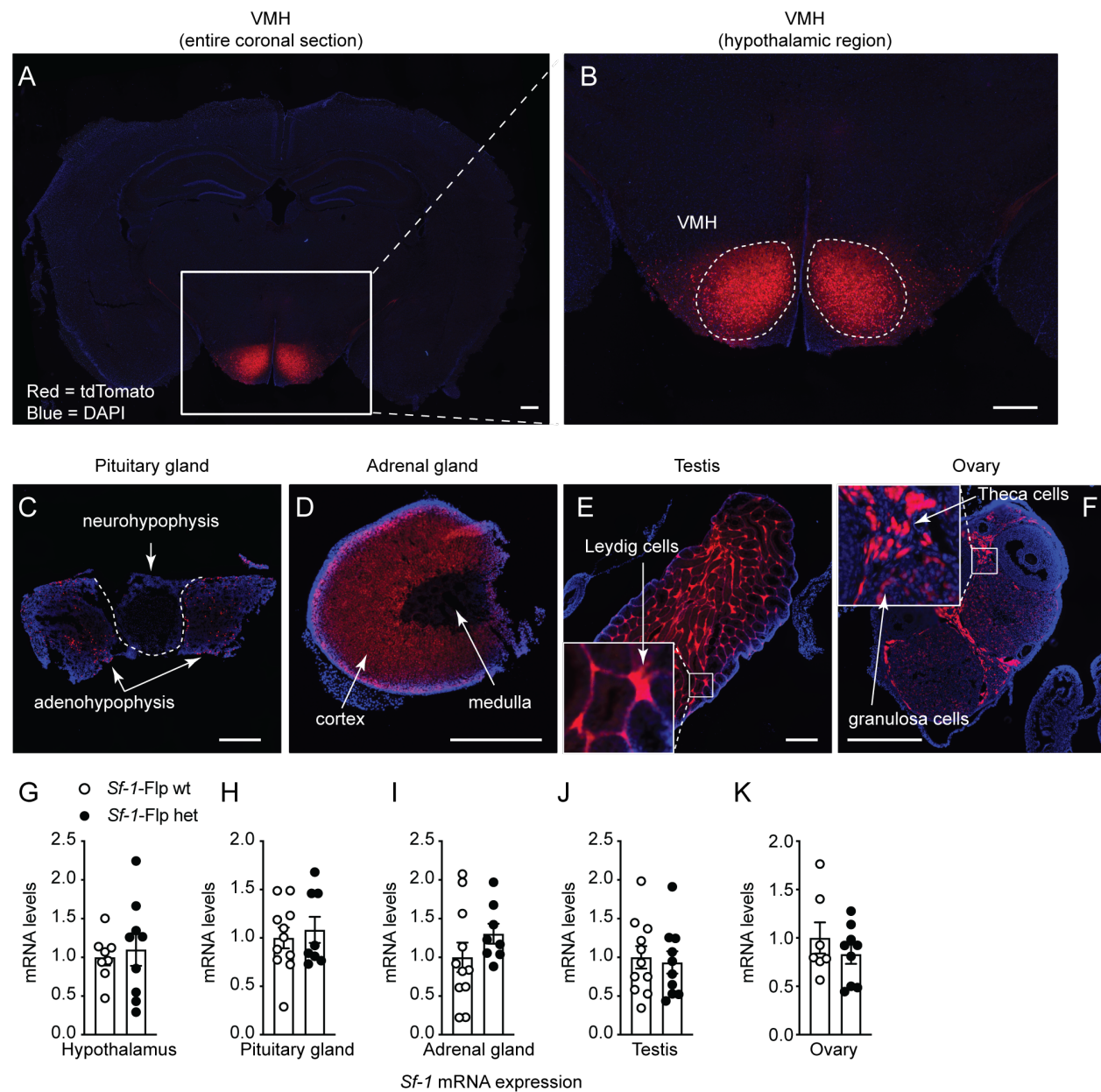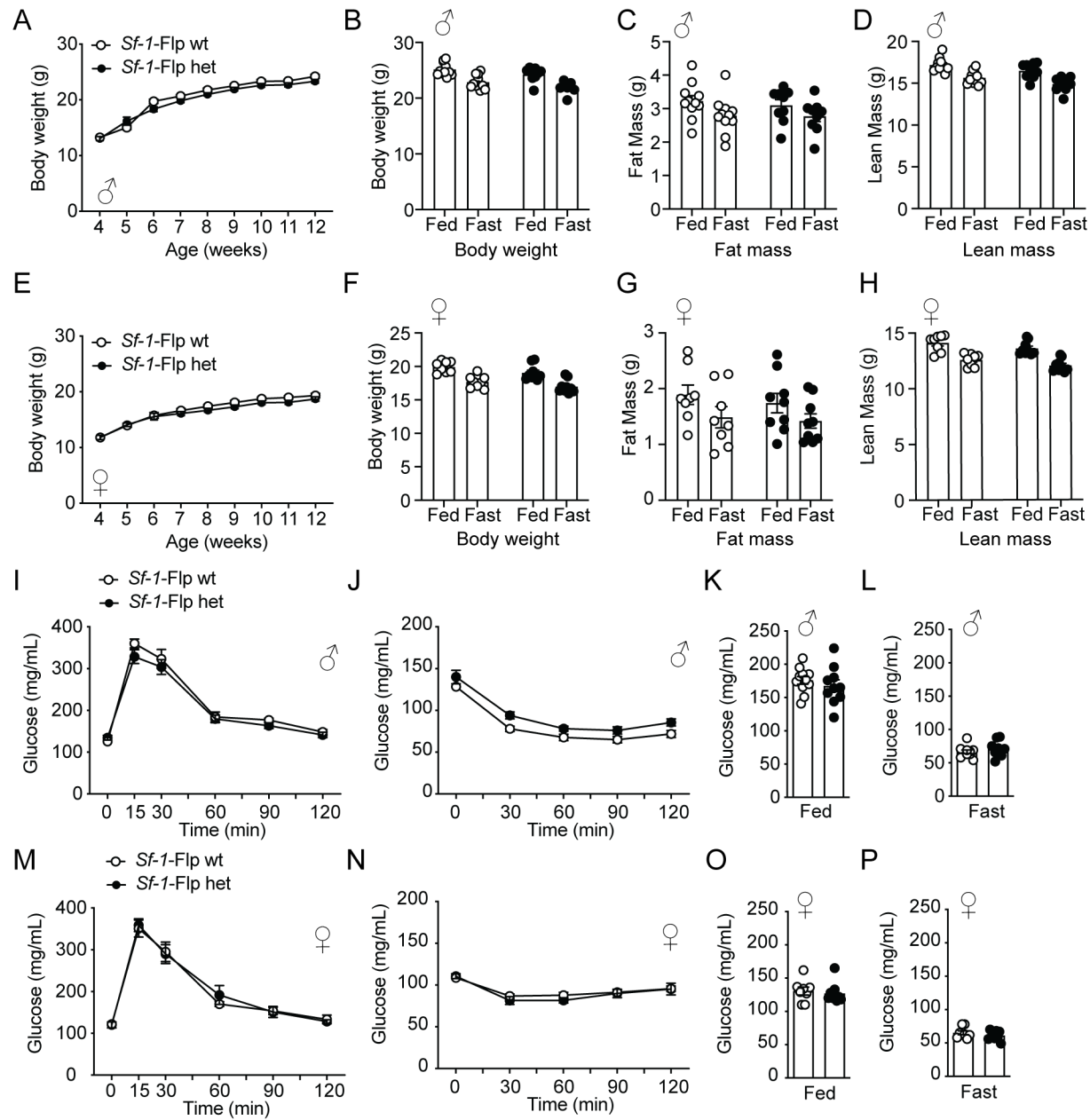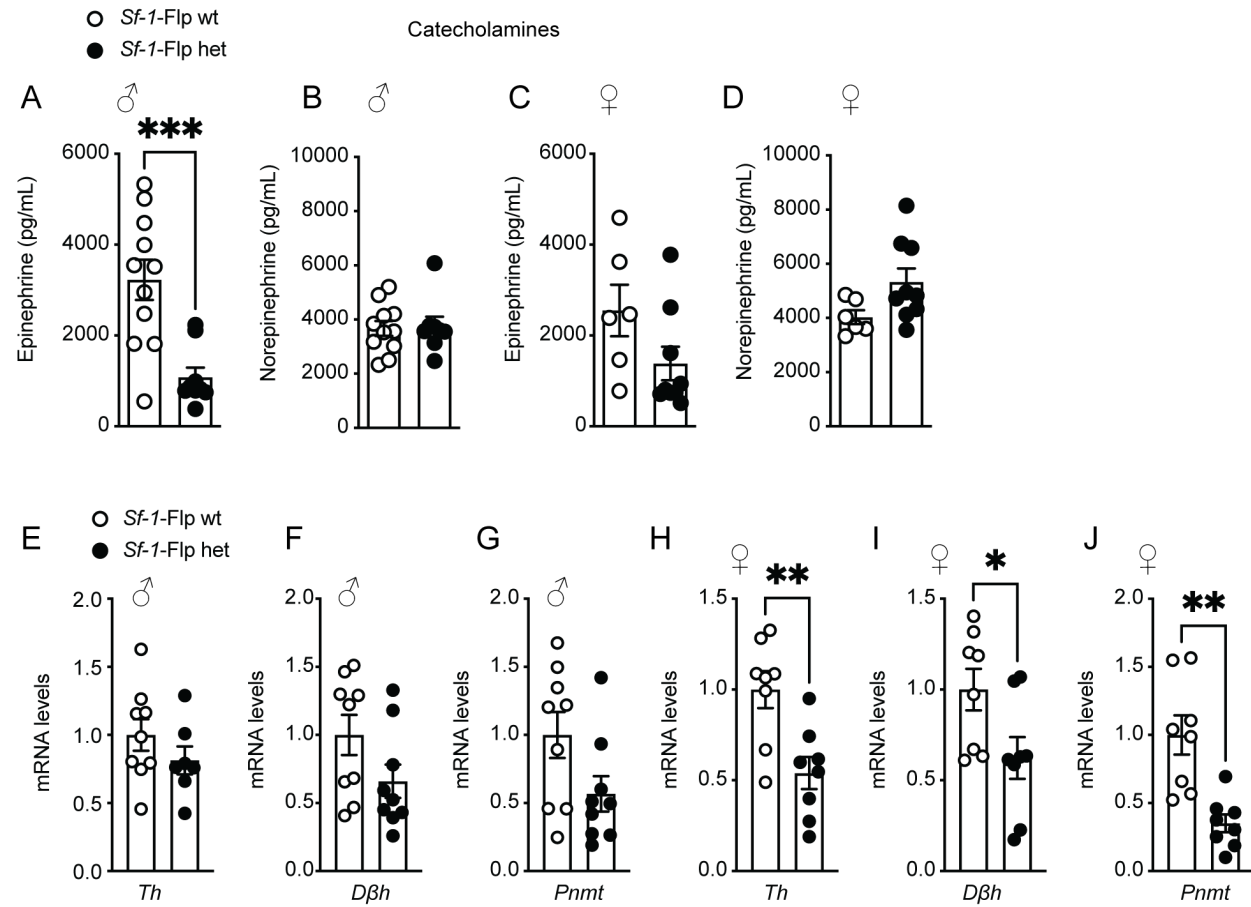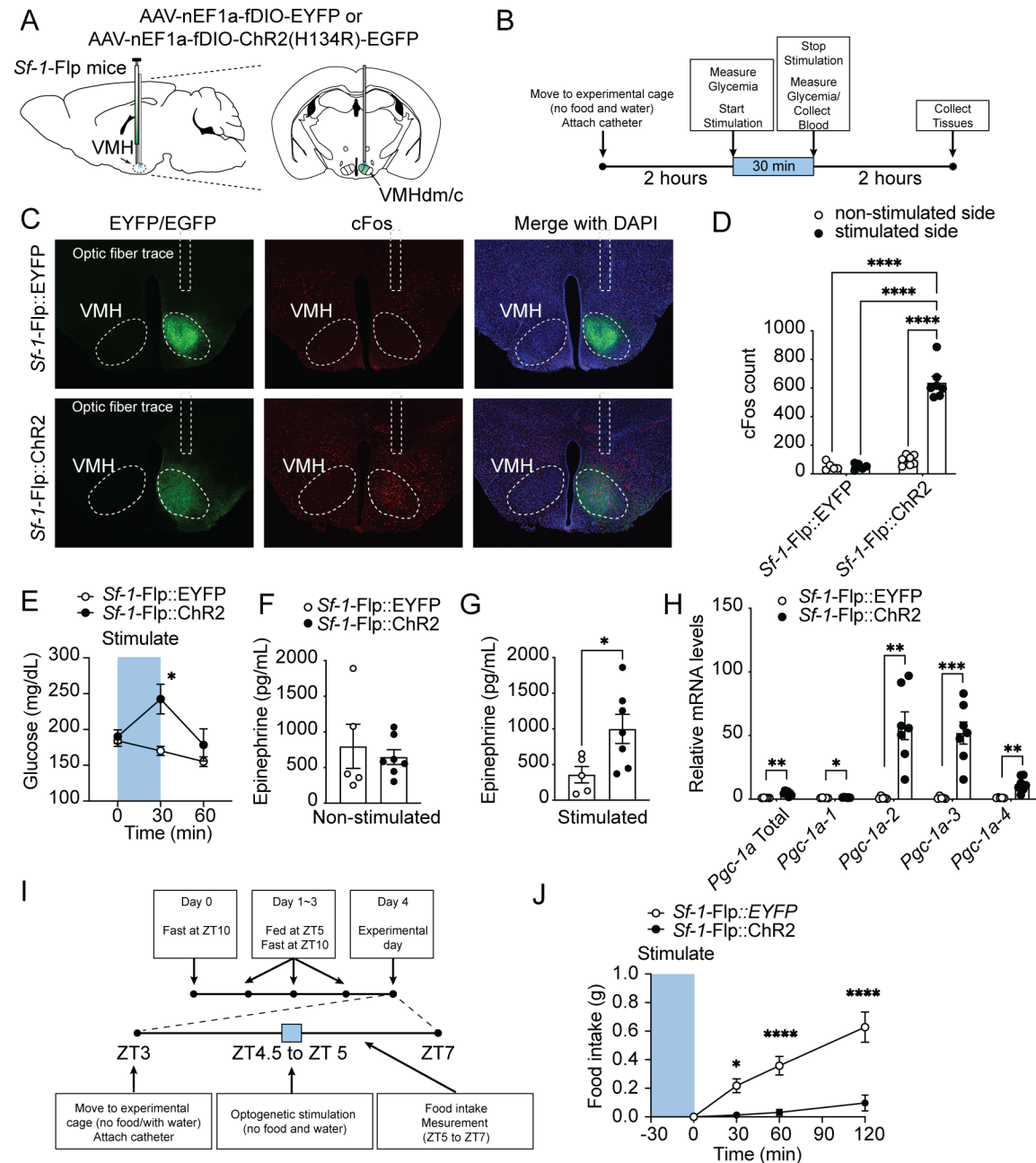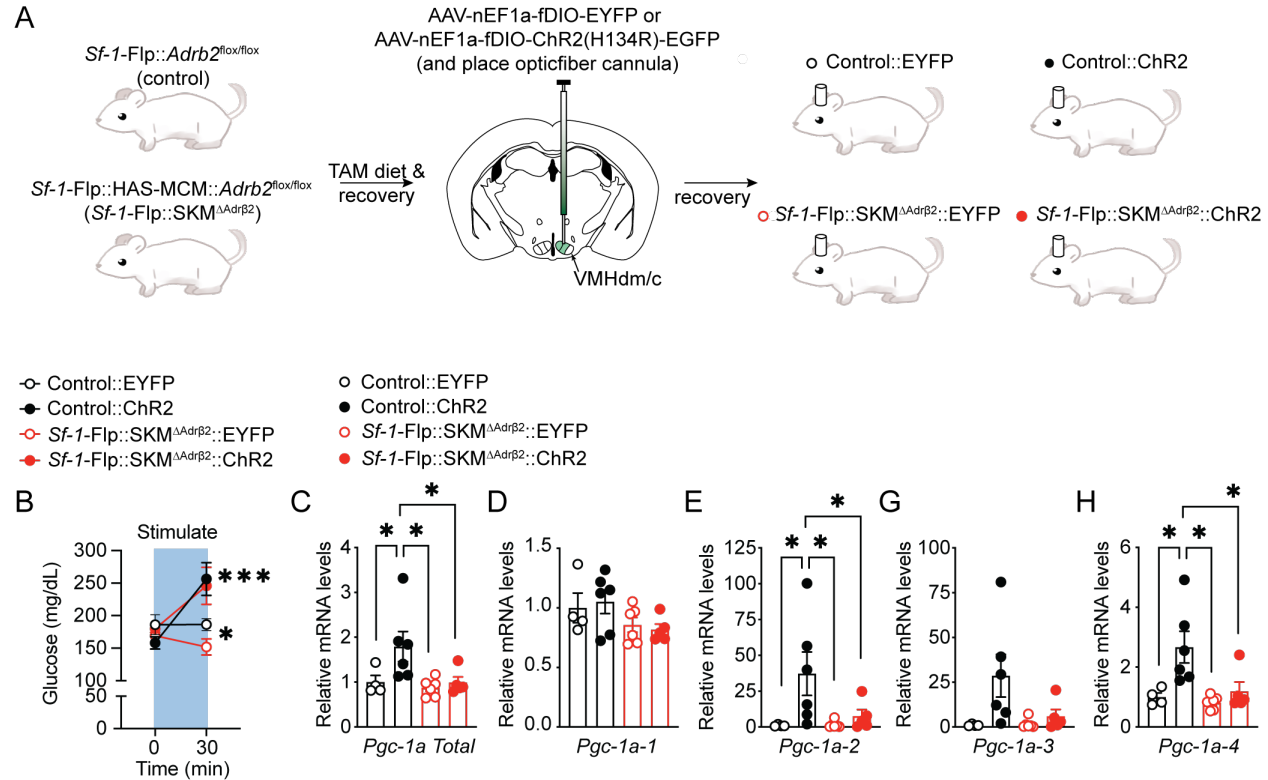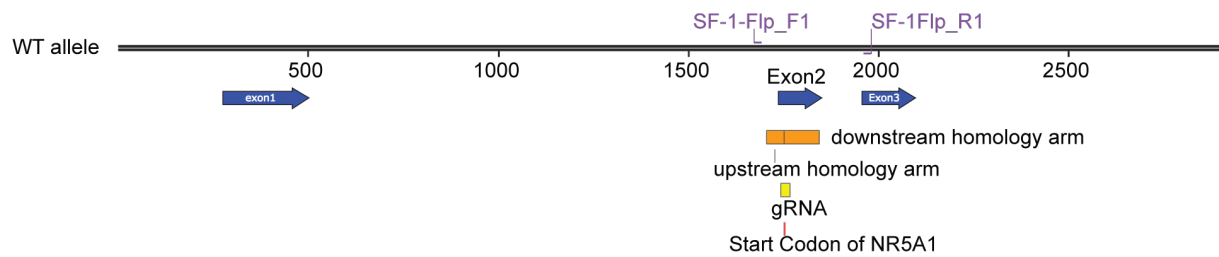
Figure 1

Figure 2

Figure 3
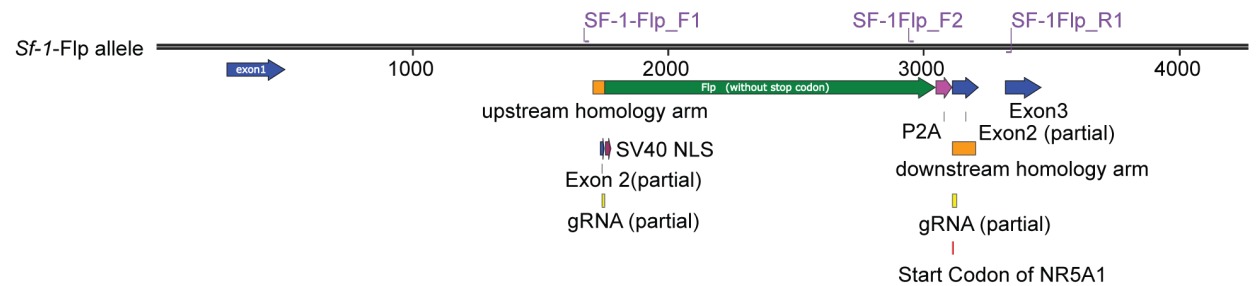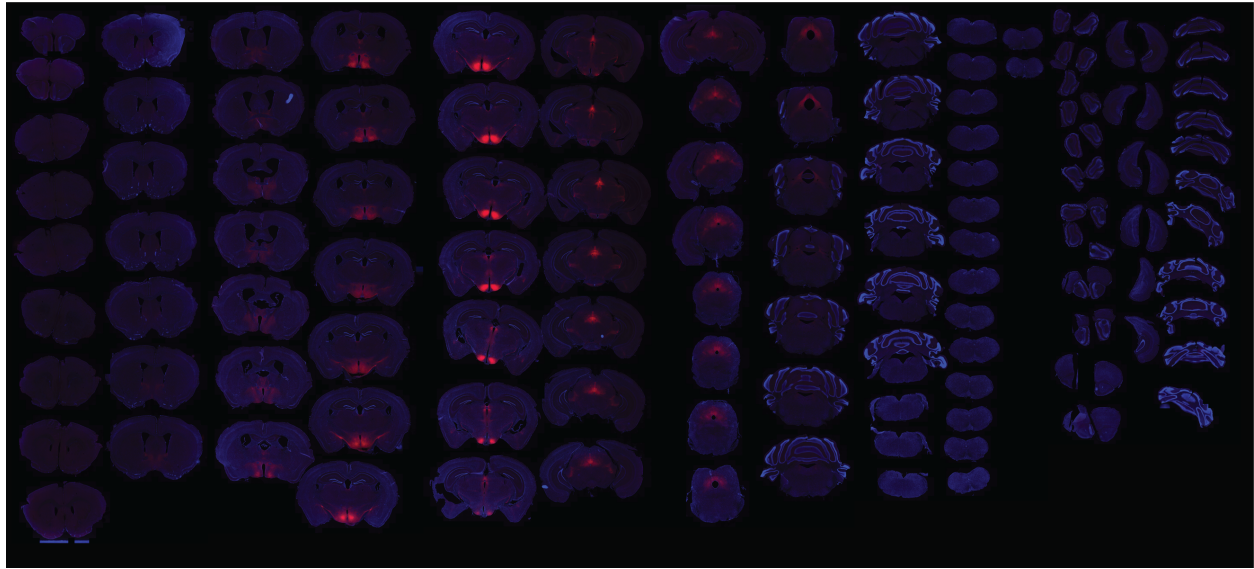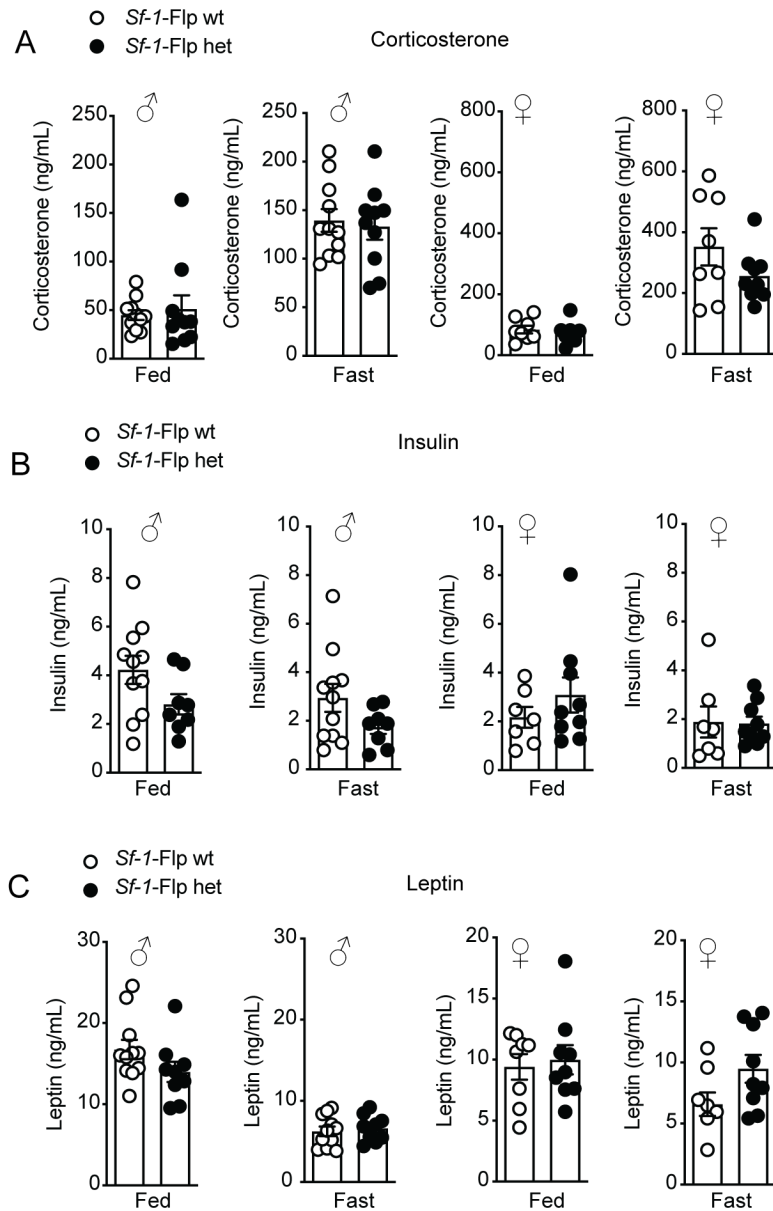
Figure 4

Figure 5

Supplemental Figure 1

Supplemental Figure 2

Supplemental Figure 3

Supplemental Figure 4

A

B